involved. In path b the potential of the Ru(IV)/(III) couple is reduced because Ru(III) is formed in a non-equilibrium proton composition. In path a the potential is reduced because of the low equilibrium concentration of the protonated oxo complex. The problem is less severe for the Ru(III)/(II) couple where the relevant p$K_a$ values are ~1 for $[Ru^{III}(bpy)_2(py)(OH_2)]^{3+}$ and ~11 for $[Ru^{II}(bpy)_2(py)(OH_2)]^{2+}$.

The "proton assisted electron transfer" or H-atom transfer pathway discussed here represents at least a partial solution to the dilemma posed by changes in proton content accompanying electron transfer. However, it is mechanistically more complex than outer-sphere electron transfer and as shown, for example, by reactions between $[Ru^{IV}(bpy)_2(py)(O)]^{2+}$ and $[Ru^{II}(bpy)_2(py)(OH_2)]^{2+}$ (eq 12) compared with $[Ru^{IV}(bpy)_2(py)(O)]^{2+}$ and $[Ru^{II}(bpy)_2(py)(OH)]^{+}$ (eq 13) or between $[Ru^{III}(trpy)(bpy)(OH)]^{2+}$ and $[Ru^{II}(bpy)_2(py)(OH_2)]^{2+}$ (eq 21) compared with $[Ru^{III}(trpy)(bpy)(OH)]^{2+}$ and $[Ru^{II}(bpy)_2(py)(OH)]^{+}$ (eq 22), will probably only play an important role for those cases where the difference between reactants is one proton and one electron, i.e., an H-atom. Where such pathways appear, as indicated by appreciable H/D kinetic isotope effects, the term "H-atom transfer" refers to what is *transferred* between reactants in the net sense and *not to the mechanism* of the event. The details of the mechanisms involved are necessarily complex, involving time dependent electronic–vibrational coupling events which demand a quantum mechanical description in the limit where the Born–Oppenheimer approximation is no longer valid.

In some cases H-atom transfer may not be competitive with an initial outer-sphere electron transfer step followed by proton transfer. H-atom transfer pathways have been invoked previously, most notably for the $[Fe(H_2O)_6]^{3+/2+}$ self-exchange reaction which displays a relatively small H/D kinetic isotope effect.[39] Although the small isotope effect can be explained as a secondary effect on an outer-sphere mechanism,[29a] there is other experimental evidence for the existence of H-atom transfer pathways. For example, although outer-sphere oxidation of $[Ru(NH_3)_6]^{2+}$ by $[Fe^{III}(H_2O)_5(OH)]^{2+}$ is decreased by $\simeq 6$ compared with $[Fe^{III}(H_2O)_6]^{3+}$, the oxidation of $[Ru(NH_3)_5(OH_2)]^{2+}$ by $[Fe(H_2O)_5(OH)]^{2+}$ is *increased* by a factor of $\simeq 6$ compared with that of $[Fe(H_2O)_6]^{3+}$.[38] While the conventional interpretation of the origin of inverse acid terms in self-exchange reactions like $[Fe(H_2O)_6]^{3+/2+}$ is attributed to an inner-sphere pathway involving the redox partners $[Fe^{III}(H_2O)_5(OH)]^{2+}$ and $[Fe^{II}(H_2O)_6]^{2+}$, there is a clear possibility that such effects could have their origin in the H-atom transfer pathway, an issue that could be resolved by further studies in $D_2O$.

**Acknowledgment** is made to the National Science Foundation for support of this research (Grant CHE-8304230) and to Prof. J. K. Beattie of the University of Sydney for helpful discussions on the kinetics analysis.

**Registry No.** $Ru^{IV}(bpy)_2(py)(O)^{2+}$, 67202-43-1; $Ru^{II}(bpy)_2(py)(OH_2)^{2+}$, 70702-30-6; $Ru^{III}(trpy)(bpy)(OH)^{2+}$, 81971-63-3; $D_2$, 7782-39-0.

(38) Meyer, T. J.; Taube, H. *Inorg. Chem.* **1968**, *7*, 2369.
(39) (a) Horne, R. A. *J. Phys. Chem.* **1960**, *64*, 1512. (b) Hudis, J.; Dodson, R. W. *J. Am. Chem. Soc.* **1956**, *78*, 911. (c) Sutin, N.; Rowley, J. K.; Dodson, R. W. *J. Phys. Chem.* **1961**, *65*, 1248. (d) Fukushima, S.; Reynolds, W. L. *Talenta* **1964**, *11*, 283.

# Electron and Energy Shuttling between Redox Sites on Soluble Polymers

**John Olmsted III,*† Steven F. McClanahan,‡ Earl Danielson,‡ Janet N. Younathan,‡ and Thomas J. Meyer*‡**

*Contribution from the Department of Chemistry and Biochemistry, California State University, Fullerton, California 92634, and the Department of Chemistry, The University of North Carolina, Chapel Hill, North Carolina 27514.* *Received November 7, 1986*

**Abstract:** 9-Methylanthracene (9-MeAn) is found to function as an efficient, sequential energy and electron transfer shuttle between chromophore and redox sites bound to separate strands of chemically modified polystyrene. Sensitized formation of the triplet excited state, $^3$(9-MeAn)*, occurs by energy transfer following visible irradiation of a polymer-bound polypyridyl complex of Ru(II), PS-($Ru^{II}$). In the presence of separate polymers containing reductive (phenothiazene, PS-PTZ) or oxidative sites (paraquat, PS-$PQ^{2+}$), a series of subsequent electron transfer steps results in the transient generation of PS-$PTZ^{+}$ and PS-$PQ^{+}$ and the net photoinduced production and separation of oxidative and reductive equivalents on separated polymers. The rate of recombination between PS-$PQ^{+}$ and PS-$PTZ^{+}$ by back electron transfer is reduced by a factor of 27 relative to an analogous system based on PTZ and $PQ^{2+}$ monomers.

Rapid "charge recombination" by back electron transfer imposes rather severe restrictions on any energy storage scheme based on electron transfer quenching of molecular excited states in solution, e.g., eq 2 followed by 3.[1] The recombination or back electron transfer step is a bimolecular process, and it is possible to reduce its rate by modifying the microenvironment of the system such that diffusion is hindered. Several approaches for making such modifications have been explored, and the results are summarized in a recent review.[2] One strategy has been to anchor the donor and acceptor sites on separate polymeric strands, thereby reducing their mobility and decreasing the rate of recombination.[2-4] However, if polymeric attachment reduces the rate of recombination, it must also slow the second-order processes by which the

$$Ru(bpy)_3^{2+} \xrightarrow{h\nu} Ru(bpy)_3^{2+*} \quad (1)$$

$$Ru(bpy)_3^{2+*} + PQ^{2+} \longrightarrow Ru(bpy)_3^{3+} + PQ^{+} \quad (2)$$

$$Ru(bpy)_3^{3+} + PQ^{+} \longrightarrow Ru(bpy)_3^{2+} + PQ^{2+} \quad (3)$$

(where bpy is 2,2′-bipyridine; $PQ^{2+}$ is paraquat,

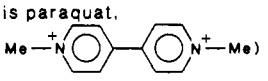


†California State University.
‡University of North Carolina.

(1) Bock, C. R.; Meyer, T. J.; Whitten, D. G. *J. Am. Chem. Soc.* **1974**, *96*, 4710.
(2) Rabani, J.; Sasson, R. E. *J. Photochem.* **1985**, *29*, 7.
(3) Sassoon, R. E.; Rabani, J. *J. Phys. Chem.* **1985**, *89*, 5500.
(4) Margerum, L. D.; Murray, R. W.; Meyer, T. J. *J. Phys. Chem.* **1986**, *90*, 7289

0002-7863/87/1509-3297$01.50/0 

photoproduced oxidative and reductive equivalents are generated.

We are interested in applications of soluble polymers in photoinduced electron transfer and report here an application based on the strategy of trapping photochemically produced oxidative and reductive redox equivalents on separate polymeric strands. Our experiments were designed to take advantage of the fact that in systems containing a sacrificial donor, 9-anthracenecarboxylate has been shown to act as an energy relay between light-absorbing sensitizers and paraquat as the final electron acceptor, eq 4 and 5.[5-7]

$$Ru(bpy)_3^{2+*} + 9\text{-}AnCO_2^- \longrightarrow Ru(bpy)_3^{2+} + {}^3(9\text{-}AnCO_2^-)^* \quad (4)$$

$$^3(9\text{-}AnCO_2^-) + PQ^{2+} \longrightarrow 9\text{-}AnCO_2^{\bullet} + PQ^{\bullet+} \quad (5)$$

(where $9\text{-}AnCO_2^-$ is 9-anthracenecarboxylate anion,

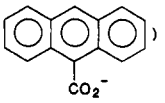

)

Because prompt recombination within the solvent cage between the anthracene–paraquat pair produced by oxidative quenching (eq 5) is spin forbidden, the separation efficiency of the redox products, $PQ^{\bullet+}$ and $9\text{-}AnCO_2^{\bullet}$, approaches unity.[8] In the systems that have been studied to date, back electron transfer has been avoided by adding reductive scavengers such as EDTA which returns the oxidized anthracene derivative to the reduced state and itself undergoes irreversible oxidation.[5] An analysis of these systems shows that the anthracene derivative plays three different roles: energy acceptor (eq 4), reducing agent as the triplet excited state (eq 5), and oxidant toward the added reductive scavenger. We have taken advantage of the energy and electron transfer capabilities of anthracene derivatives to develop a three-component, polymer-based photoredox system. In this system, 9-methylanthracene (9-MeAn) is used to transfer the excited state energy of an initially excited chromophoric site as transiently stored oxidative and reductive equivalents on separate polymeric strands.

## Experimental Section

**Materials.** The polymeric compounds employed in this study (Figure 1) are comprised of a 1:1 copolymer of styrene and chloromethylstyrene. The method of Arshady, Reddy, and George[9] was used to copolymerize the monomers styrene and chloromethylstyrene with AIBN in chlorobenzene to obtain a copolymer with an average molecular weight of 7800 as determined by gel permeation chromatography with polystyrene standards. The redox and chromophoric sites are chemically bound by nucleophilic substitution of $Cl^-$ with a reproducible loading stoichiometry, $x$, determined by $^1H$ NMR and elemental analysis. For our samples, $x$ denotes the number of chromophore or redox sites chemically bound per "average" polymer strand which consists of ~30 chloromethylated sites. The syntheses of polymers **1** and **2** containing bound PTZ and $PQ^{2+}$ has been previously described.[10] Preparation of polymer **3** will be detailed in a separate paper which is currently in preparation.

9-Methylanthracene (Aldrich) was recrystallized three times from ethanol. 10-Methylphenothiazene was recrystallized from toluene and stored protected from light.

Transient spectroscopic studies of the rates for the various shuttle and recombination reactions were carried out in dimethylformamide (Burdick and Jackson) acidified with 1 drop of $HClO_4$ (70%) per 15 mL of solution. Solutions were thoroughly bubble-deaerated with argon and were maintained under an argon blanket during experiments.

**Table I.** Rate Constants for the Energy and Electron Transfer Processes in Acidified DMF at Room Temperature

| reaction | $k' \times 10^{-5}$ $s^{-1}$ | $k \times 10^{-9}$ $M^{-1}\ s^{-1}$ |
|---|---|---|
| 9-MeAn + PS-$(Ru^{II})_2(Ru^{II*})$ → $^3$(9-MeAn)* + PS-$(Ru^{II})_3$ | 36.0 | 2.0 |
| $^3$(9-MeAn)* + PS-$(PQ^{2+})_9$ → (9-MeAn)$^{\bullet-}$ + PS-$(PQ^{2+})_8(PQ^{\bullet+})$ | 3.8 | 5.3 |
| (9-MeAn)$^{\bullet+}$ + PS-$(PTZ)_5$ → 9-MeAn + PS-$(PTZ)_4(PTZ^{\bullet+})$ | 3.8 | 5.3 |
| (9-MeAn)$^{\bullet+}$ + PS-$(PTZ)_5$ → 9-MeAn + PS-$(PTZ)_4(PTZ^{\bullet+})$ | 2.2 | 3.0 |
| PS-$(PTZ)_4(PTZ^{\bullet+})$ + PS-$(PQ^{2+})_8(PQ^{\bullet+})$ → PS-$(PTZ)_5$ + PS-$(PQ^{2+})_9$ | | 0.10 |

**Table II.** Recombination Rate Constants in Acidified DMF at Room Temperature Determined by Conventional Flash Photolysis[a]

| reaction | $k \times 10^{-9}$ $M^{-1}\ s^{-1}$ |
|---|---|
| $PTZ^{\bullet+} + PQ^{\bullet+} \rightarrow PTZ + PQ^{2+}$ | 2.7 |
| PS-$(PTZ)_4(PTZ)^{\bullet+} + PQ^{\bullet+} \rightarrow$ PS-$(PTZ)_5 + PQ^{2+}$ | 1.1 |
| $PTZ^{\bullet+}$ + PS-$(PQ^{2+})_8(PQ^{\bullet+}) \rightarrow PTZ$ + PS-$(PQ^{2+})_9$ | 0.41 |
| PS-$(PTZ)_4(PTZ^{\bullet+})$ + PS-$(PQ^{2+})_8(PQ^{\bullet+}) \rightarrow$ PS-$(PTZ)_5$ + PS-$(PQ^{2+})_9$ | 0.10 |

[a] The rate constant data were obtained by monitoring the transient absorbance behavior following conventional flash photolysis of solutions containing $Ru(bpy)_3^{2+}$ as sensitizer and the PTZ or $PQ^{2+}$ forms of the quenchers. Note, for example, eq 1–3.

**Equipment.** Conventional flash photolysis studies were conducted with a standard flash lamp apparatus.[11a,b] Transient absorbance spectra were conducted with a Quanta-Ray DCR-2A Nd:YAG laser pumping coumarin 460 dye in a PDL-2 dye laser producing an excitation pulse of ~6 ns at 5 mJ/pulse. The probe beam, at right angle to the excitation beam, was provided by a pulsed Osram XBO 150 W xenon arc lamp contained in a PRA LH215 housing. Electronic control and synchronization of the laser and probe was provided by electronics of our own design. The absorption signals were collected with quartz optics (f 3.5) with suitable aperture stops, imaged onto the slit of 0.5 M (f 3.4) grating monochromator, and detected with a Hamamatsu R446 5 stage PMT coupled to a Tektronix 7912AD digitizer interfaced to a DEC PDP11/34 minicomputer.

## Results

Figure 2a shows the transient absorbance changes observed at 517 and 610 nm following visible flash photolysis of an acidified DMF solution containing $Ru(bpy)_3^{2+}$, $PQ^{2+}$, and 10-methylphenothiazene (PTZ). Absorbance maxima occur for $PTZ^{\bullet+}$ at 517 nm and for $PQ^{2+}$ at 610 nm, and the decreases observed are consistent with back electron transfer (eq 7) following optical excitation (eq 1), oxidative quenching (eq 2), and capture of $Ru(bpy)_3^{3+}$ by PTZ (eq 6) as observed in related systems.[12,13] The net effect of the quenching and electron transfer steps in eq 1, 2, and 6 is to convert the excited state energy in $Ru(bpy)_3^{2+*}$ (2.1 eV) into transiently stored redox energy as $PQ^{\bullet+}$ and $PTZ^{\bullet+}$ (1.1 eV).

$$Ru(bpy)_3^{3+} + PTZ \rightarrow Ru(bpy)_3^{2+} + PTZ^{\bullet+} \quad (6)$$

$$PTZ^{\bullet+} + PQ^{+} \rightarrow PTZ + PQ^{2+} \quad (7)$$

Figure 2b depicts the results of visible flash photolysis under the same conditions but with the chromophore, quencher, and phenothiazene sites chemically bound as PS-$(Ru^{2+})_3$, PS-$(PQ^{2+})_9$, and PS-$(PTZ)_5$. When the chromophore and quencher sites are bound to the less mobile polymeric units, no transient signals are observed since under these conditions electron transfer quenching

(5) Johansen, O.; Mau, A. W.-H.; Sasse, W. H. F. *Chem. Phys. Lett.* **1983**, *94*, 113.
(6) Edel, A.; Marnot, P. A.; Sauvage, J. P. *Nouv. J. Chim.* **1984**, *8*, 495.
(7) Mau, A. W.-H.; Johansen, O.; Sasse, W. H. F. *Photochem. Photobiol.* **1985**, *41*, 503.
(8) Olmsted, J., III; Meyer, T. J. *J. Phys. Chem.*, in press.
(9) Arshady, R.; Reddy, B. S. R.; George, M. H. *Polymer* **1984**, *25*, 716.
(10) Margerum, L. D.; Murray, R. W.; Meyer, T. J. *J. Phys. Chem.* **1986**, *90*, 2696.
(11) (a) Young, R. C.; Keene, F. R.; Meyer, T. J. *J. Am. Chem. Soc.* **1977**, *99*, 2468. (b) Appropriate filters were employed to prevent irradiations higher in energy than 430 nm; the apparatus was modified to optically trigger the oscilloscope.
(12) Young, R. C.; Meyer, T. J.; Whitten, D. G. *J. Am. Chem. Soc.* **1975**, *97*, 4781.
(13) The same net products appear via initial reductive quenching, $Ru(bpy)_3^{2+*}$ + PTZ → $Ru(bpy)_3^{+}$ + $PTZ^{\bullet+}$, followed by capture of $Ru(bpy)_3^{+}$ by $PQ^{2+}$, $Ru(bpy)_3^{+} + PQ^{2+} \rightarrow Ru(bpy)_3^{2+} + PQ^{\bullet+}$. The quenching rate constants by $PQ^{2+}$ and PTZ are known (ref 1 and 4), and the distribution between the two pathways depends on the relative concentrations of the two quenchers.

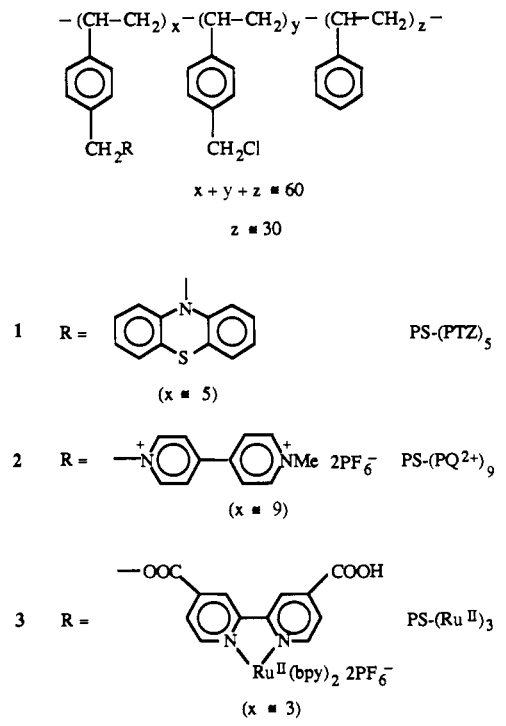


**Figure 1.** Structures and abbreviations of the chromophore and redox polymers.

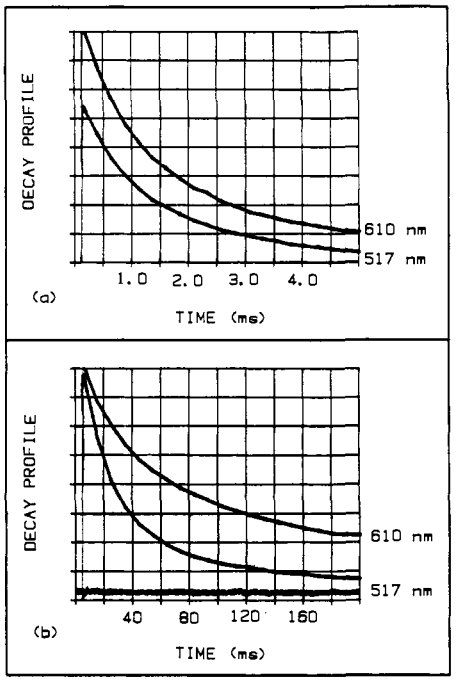


**Figure 2.** The results of conventional visible flash photolysis in acidified DMF solutions containing (a) $[Ru(bpy)_3^{2+}](PF_6)_2$ ($o.d._{450\ nm}$ = 0.1), $PQ^{2+}(PF_6)_2$ (0.13 mg/mL), and 10-MePTZ (0.46 mg/mL); and (b) PS-$(Ru^{II})_3$ ($o.d._{450\ nm}$ = 0.1), PS-$(PQ^{2+})_9$ (0.2 mg/mL), and PS-$(PTZ)_5$ (0.14 mg/mL). Base line is in the absence of the 9-MeAn shuttle. As shown, absorbance decays are monitored at $\lambda_{max}$ for $PTZ^{\bullet+}$ (517 nm) and for $PQ^+$ (610 nm) with the addition of 2 mM 9-MeAn shuttle.

is not competitive with excited state decay. However, upon addition of 2 mM 9-MeAn, the transient decay behavior associated with back electron transfer between $PTZ^{\bullet+}$ and $PQ^+$ reappears but on a considerably longer time scale than in the all-monomer system (Table II). The Ru(II)-based metal to ligand charge transfer excited state (MLCT)[14] in which the excited electron is

(14) (a) Kalyanasundaram, K. *Coord. Chem. Rev.* **1982**, *46*, 159. (b) Meyer, T. J. *Pure Appl. Chem.* **1986**, *25*, 2357.

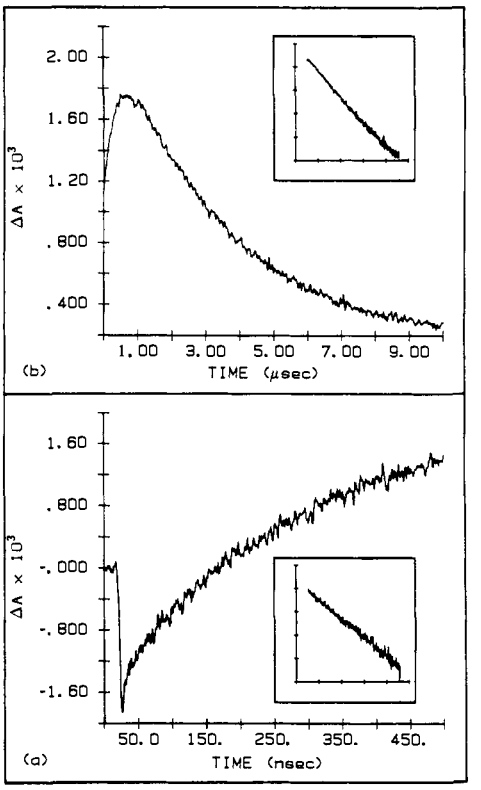


**Figure 3.** Transient absorbance changes and first order ln $(A_t - A_\infty)$ vs. time kinetic plots (as inserts) showing (a) the growth and (b) the decay of $^3$(9-MeAn)* at 430 nm following 460 nm laser flash photolysis of an acidified DMF solution containing PS-$(Ru^{II})_3$ ($o.d._{450\ nm}$ = 0.1), PS-$(PQ^{2+})_9$ (0.2 mg/mL), PS-$(PTZ)_5$ (0.14 mg/mL), and 9-MeAn (0.42 mg/mL).

localized largely on the electron deficient 4,4′-diacid ester bipyridyl ring is quenched, essentially completely, by 9-MeAn under these conditions, eq 8.

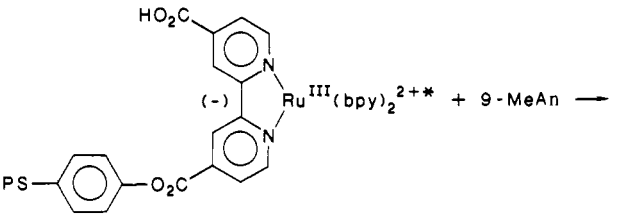


$$[4\text{-}(CO_2\text{-}p\text{-}PS\text{-}C_6H_4)\text{-}4'\text{-}(CO_2H)bpy]Ru(bpy)_2^{2+} + {}^3(9\text{-MeAn})^* \quad (8)$$

By using the shorter time scale (~6 ns compared to ~15 μs) of the laser pulse, it is possible to follow directly the sequence of events leading to the separated $PQ^{\bullet+}$ and $PTZ^{\bullet+}$ sites in the polymer-containing solutions. In figure 3a is shown the transient absorption changes that occur following 460-nm excitation of a solution of the same composition as in Figure 2b. At 430 nm a rapid increase is observed which follows first-order kinetics (Figure 2a). This transient signal at 430 nm arises from triplet–triplet absorption by $^3$(9-MeAn)* based on the appearance of a similar absorption feature following direct excitation of 2 mM 9-MeAn in acidified DMF. The triplet state is relatively long-lived (ms), its actual lifetime being determined by self-quenching and the presence of trace impurities, in particular oxygen. The observed behavior is consistent with the energy transfer step

$$PS\text{-}(Ru^{II})_2(Ru^{II*}) + 9\text{-MeAn} \rightarrow PS\text{-}(Ru^{II})_3 + {}^3(9\text{-MeAn})^* \quad (9)$$

The subsequent decay of $^3$(9-MeAn)* (Figure 3b) on a slower time scale is paralleled by the rate of appearance of PS-$PQ^{\bullet+}$

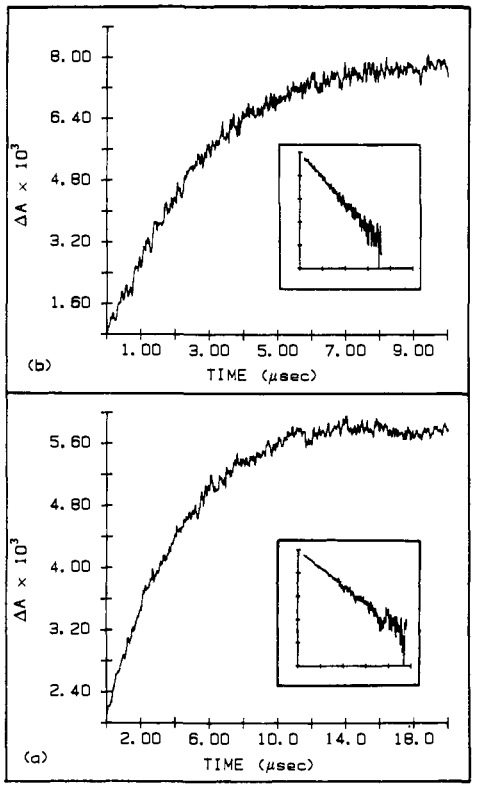


**Figure 4.** Transient absorbance changes and first order ln $(A_0 - A_t)$ vs. time kinetic plots (as inserts) following 460 nm laser excitation demonstrating (a) the growth of PS-PTZ$^{\bullet+}$ at 515 nm and (b) the growth of PS-PQ$^{\bullet+}$ at 610 nm in an acidified DMF solution containing PS-$(Ru^{II})_3$ ($o.d._{450\ nm}$ = 0.1), PS-$(PQ^{2+})_9$ (0.2 mg/mL), PS-$(PTZ)_5$ (0.14 mg/mL), and 9-MeAn (0.42 mg/mL).

monitored at 610 nm (Figure 4b) showing that the next step is oxidative quenching of $^3$(9-MeAn)* by PS-$PQ^{2+}$

$$PS\text{-}(PQ^{2+})_9 + {}^3(9\text{-MeAn})^* \rightarrow PS\text{-}(PQ^{2+})_8(PQ^{\bullet+}) + 9\text{-MeAn}^{\bullet+} \quad (10)$$

On a still longer time scale, and subsequent to the appearance of $PQ^{\bullet+}$, an absorbance increase is observed at 515 nm corresponding to the growth of $PTZ^{\bullet+}$ via

$$9\text{-MeAn}^{\bullet+} + PS\text{-}(PTZ)_5 \rightarrow 9\text{-MeAn} + PS\text{-}(PTZ)_4(PTZ^{\bullet+}) \quad (11)$$

Evidence for the separate series of quenching and electron transfer reactions in eq 1–11 can also be obtained by laser flash photolysis. When a thoroughly deaerated solution of polystyrene-bound ruthenium and 9-methylanthracene is excited with a 460-nm laser pulse, the triplet–triplet absorption maximum for $^3$(9-MeAn)* is observed at 435 nm (Figure 3a). Addition of polystyrene-bound paraquat to this solution results in quenching of the triplet absorbance and appearance of a new transient absorbance at 610 nm corresponding to $PQ^{\bullet+}$. The later absorbance is quenched, in turn, by the addition of polystyrene-bound phenothiazene. Although in principle it should be possible to initiate the sequence of electron transfer events by direct excitation of 9-MeAn, in practice the sensitized reaction is more efficient since it gives $^3$(9-MeAn)* directly. The kinetic results obtained following UV photolysis are also complicated by UV-induced photodegradation of PS-$(PTZ)_5$.

Analysis of the transients shown in Figures 3 and 4 yields pseudo-first-order rate constants that can be converted into second-order rate constants with use of the concentration of the quenching species which are present in pseudo-first-order excess. Rate constants for the various processes are collected in Table I. For the quenching of $^3$(9-MeAn)* by PS-$(PQ^{2+})_9$, the rate constant determined by monitoring either anthracene triplet decay

**Scheme I**

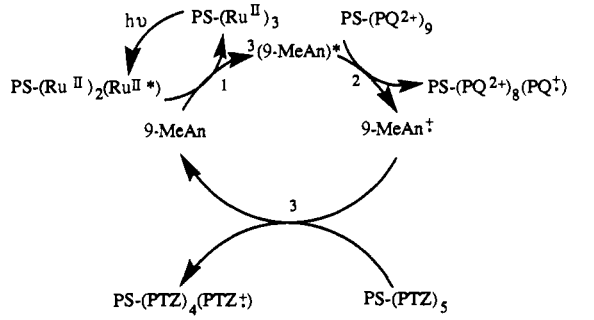


or paraquat radical cation growth at two different concentrations of PS-$(PQ^{2+})_9$ gave results that were the same within ±10%. From the data in Table I, the rate constants for the initial energy transfer step and the two following electron transfer steps are comparable. The ability to discriminate among them temporally as in Figures 3 and 4 relies on setting the relative concentrations of the components involved—9-MeAn in eq 7, PS-$(PQ^{2+})_9$ in eq 8, and PS-$(PTZ)_5$—in the proper order.

When the series of shuttle processes in eq 9–11 is complete, the products are a pair of polymer-bound radical cations on separate polymer units, PS-$(PQ^{2+})_8(PQ^{\bullet+})$ and PS-$(PTZ)_4$-$(PTZ^{\bullet+})$. They ultimately recombine by electron transfer to return the system to its initial state. The recombination step is a second-order process that is strongly affected by polymer binding. We have measured rates of recombination for various combinations of polymer-bound and monomeric donors and acceptors, based on PTZ and $PQ^{2+}$ by conventional flash photolysis, e.g., Figure 2b. Second-order recombination rate constants for a series of reactions are given in Table II. In all cases the reactions followed second-order equal concentration kinetics for at least 2–3 half-lives as predicted, for example, for a series of reactions like eq 1–3.

## Discussion

This work has demonstrated that through a series of energy and electron transfer reactions, 9-methylanthracene can convert the initially stored MLCT excited state energy of PS-$(Ru^{II})_2$-$(Ru^{II}*)$ into transiently stored oxidative and reductive redox equivalents on separated polymeric units. The series of reactions that enable 9-MeAn to act as a successful shuttle is illustrated in Scheme I. Each of the individual steps 1, 2, and 3 shown in the scheme is energy sufficient as evidenced by the relative energies of the Ru(II)-based state (2.1 eV) and $^3$(9-MeAn)* (1.79 eV),[15] the redox potentials for the PS-$(PQ)_8(PQ^{2+/+})$ and estimated triplet excited state redox couples $^3$(9-MeAn)$^{*+/0}$ (–0.31 V[10] and ~0.61 V vs. the sodium saturated calomel electrode (SSCE)), and the potentials for the PS-$(PTZ)_4(PTZ)^{+/0}$ and (9-MeAn)$^{*+/0}$ couples (0.78 V[10] and 1.18 V[16] vs. SSCE, respectively).

Although we have not made quantum yield measurements, if the energy transfer efficiency in eq 11 is unity as it is for 9-$AnCO_2^-$ and $Ru(bpy)_3^{2+*}$ in water,[5] the efficiency of the net energy conversion process

$$PS\text{-}(Ru^{II})_2(Ru^{II}*) + PS\text{-}(PQ^{2+})_9 + PS\text{-}(PTZ)_5 \rightarrow PS\text{-}(Ru^{II})_3 + PS\text{-}(PQ^{2+})_8(PQ^{\bullet+}) + PS\text{-}(PTZ)_4(PTZ^{\bullet+}) \quad (12)$$

could be as high as unity as well. Another advantage of the system as a transient charge storage device is the relatively hindered rate for back electron transfer which is comparable to that reported by Sassoon and Rabani for donor–acceptor charge pairs bound to polyelectrolytes.[3] Electrostatic effects as well as the relatively limited mobility of the polymeric units may play a role in our system, as it does in theirs, in restricting collisions between charged species. The importance of electrostatic effects is illustrated by the decreased recombination rate constant (~3-fold) for the reaction between PS-$(PQ^{2+})_8(PQ^{\bullet+})$ and $PTZ^{\bullet+}$ compared to the

(15) Evans, D. F. *J. Chem. Soc.* **1957**, 1351.
(16) The redox potential was obtained in deaerated $CH_3CN$ containing 0.1 M $Et_4NClO_4$.

reaction between $PQ^{\bullet+}$ and PS-$(PTZ)_4(PTZ^{\bullet+})$ (Table II) where electrostatic repulsion is considerably less. The importance of electrostatic effects is also suggested by qualitative observations which show that the recombination rate for the polymer bound species can increase dramatically with increasing ionic strength.

In the three-polymer system, the reduced acceptor, PS-$PQ^{\bullet+}$, is stable under the conditions of the experiment. However, when no added donor PTZ is present in the solution, 9-$MeAn^{\bullet+}$ undergoes an irreversible reduction that removes it from the system. Addition of PTZ at high enough concentrations to intercept 9-$MeAn^{\bullet+}$ before it decomposes leads to a considerably enhanced stability.

**Acknowledgment.** This research was supported by grants from the National Science Foundation (Grant no. CHE-8503092) and the Army Research Office, Durham. J.O. acknowledges California State University for a sabbatical leave and the University of North Carolina for a visiting appointment for the time period which this work was performed.

**Registry No.** 9-Me-An, 779-02-2.

# Electronic Structure of Low-Spin Ferric Porphyrins: A Single-Crystal EPR and Structural Investigation of the Influence of Axial Ligand Orientation and the Effects of Pseudo-Jahn–Teller Distortion

**Robert Quinn, Joan Selverstone Valentine,* Marianne P. Byrn, and Charles E. Strouse***

*Contribution from the Department of Chemistry and Biochemistry, the J. D. McCullough X-ray Crystallography Laboratory, and the Solid State Science Center, University of California, Los Angeles, California 90024.* *Received September 19, 1986*

**Abstract:** X-ray structure determinations are reported for the (tetraphenylporphyrinato)iron(III) complexes of the substituted imidazole ligands *cis*- and *trans*-methylurocanate (cMU and tMU, respectively). Both complexes are six-coordinate and low-spin. The cMU ligand has an internal hydrogen bond, while the tMU ligand is hydrogen bonded to a THF solvate molecule. Crystals of the cMU complex contain two crystallographically independent centrosymmetric cations; these species differ in the orientation of the imidazole ligands with respect to the porphyrin. Single-crystal EPR **g**-tensor determinations for the two forms of the cMU complex reveal that the ligand orientation influences both the distribution of spin density in the complex and the energies of the highest occupied molecular orbitals. This influence appears to arise in part from the direct interaction between metal and axial ligand $\pi$ orbitals and in part through pseudo-Jahn–Teller induced distortion of the porphyrin ligand. Crystal data: $FeTPP(cMU)_2SbF_6 \cdot 1.5$toluene, space group $P\bar{1}$, $Z = 2$, $a = 10.406$ (5) Å, $b = 11.752$ (4) Å, $c = 28.538$ (10) Å, $\alpha = 103.34$ (3)°, $\beta = 108.35$ (3)°, $\gamma = 106.18$ (3)° at 115 K; $FeTPP(tMU)_2SbF_6 \cdot 2THF$, space group $P\bar{1}$, $Z = 1$, $a = 9.898$ (3) Å, $b = 12.600$ (4) Å, $c = 15.344$ (8) Å, $\alpha = 99.99$ (3)°, $\beta = 112.82$ (3)°, $\gamma = 114.58$ (2) at 115 K.

The common occurrence of histidine as an axial ligand in heme proteins has prompted the synthesis of numerous analogues designed to explore the role of this ligand in heme chemistry. Several aspects of the imidazole–heme interaction have attracted attention. Substitution and hydrogen bonding induced changes in ligand basicity have been explored spectroscopically and electrochemically.[1,2] EPR characterization of the electronic structure has been particularly useful in this regard. X-ray structural investigations have indicated that changes in the orientation of the axial ligands with respect to the porphyrin affect the Fe–N bond lengths and the thermodynamic stability.[3] It appears that in some situations this effect is sufficient to alter the spin state of the complex.[4] The influence of the relative orientations of two axial ligands on the spectroscopic and electrochemical properties has also been discussed.[5] The structural investigations reported herein were initiated to characterize the hydrogen bonding in two isomeric iron(III)–imidazole complexes. The occurrence of two conformers in the crystal structure of one of these complexes has been exploited through single-crystal **g**-tensor determination. This determination has provided a detailed picture of the ways in which the orientation of the axial ligands with respect to the porphyrin ligand influences the electronic structure.

The observation that the histidyl imidazole ligands of hemoproteins are usually hydrogen bonded to another group on the protein[6] has led to the hypothesis that such hydrogen bonding might alter the chemical properties of the heme moiety.[1] Coordination of imidazolate, the limit of strongly hydrogen bonded imidazole, leads to ferric porphyrin complexes with properties quite different from those of the analogous imidazole complexes.[7,8] Differences in the IR and electrochemical properties of a series of complexes of the form $FeTPP(L)_2SbF_6$[9] where L is imidazole or a substituted imidazole have demonstrated that the mode of hydrogen bonding to coordinated imidazole has a substantial effect on these properties.[1] Included in this series were two new imidazole complexes in which the isomeric ligands, *cis*-methylurocanate

(1) Quinn, R.; Mercer-Smith, J.; Burstyn, J. N.; Valentine, J. S. *J. Am. Chem. Soc.* **1984**, *106*, 4136–4144.
(2) Walker, F. A.; Reis, D.; Balke, V. L. *J. Am. Chem. Soc.* **1984**, *106*, 6888–6898.
(3) Scheidt, W. R.; Chipman, D. M. *J. Am. Chem. Soc.* **1986**, *108*, 1163–1167.
(4) Geiger, D. K.; Lee, Y. J.; Scheidt, W. R. *J. Am. Chem. Soc.* **1984**, *106*, 6339–6343.
(5) Walker, F. A.; Huynh, B. H.; Scheidt, W. R.; Osvath, S. R. *J. Am. Chem. Soc.* **1986**, *108*, 5288–5297.
(6) Valentine, J. S.; Sheridan, R. P.; Allen, L. C.; Kahn, P. C. *Proc. Natl. Acad. Sci. U.S.A.* **1979**, *76*, 1009–1013.
(7) Quinn, R.; Nappa, M.; Valentine, J. S. *J. Am. Chem. Soc.* **1982**, *104*, 2588–2595.
(8) Quinn, R.; Strouse, C. E.; Valentine, J. S. *Inorg. Chem.* **1983**, *22*, 3934–3940.
(9) Abbreviations used are as follows: TPP, tetraphenylporphinato; tMU, *trans*-methylurocanate; cMU *cis*-methylurocanate; ImH, imidazole; 2MeImH, 2-methylimidazole; 1MeIm, 1-methylimidazole; P, porphyrin; L, ligand; EPR, electron paramagnetic resonance; THF, tetrahydrofuran; OAc, acetate; OEP, octaethylporphinato.

0002-7863/87/1509-3301$01.50/0 